bioRxiv preprint doi: https://doi.org/10.1101/441659; this version posted August 5, 2019. The copyright holder for this preprint (which was not certified by peer review) is the author/funder, who has granted bioRxiv a license to display the preprint in perpetuity. It is made available under aCC-BY-NC-ND 4.0 International license.

Diffusion Tensor Model links to Neurite Orientation Dispersion and Density Imaging at high b-value in Cerebral Cortical Gray Matter

Authors:

Hikaru Fukutomi[1,2], Matthew F. Glasser[3,4], Katsutoshi Murata[5], Thai Akasaka[2], Koji Fujimoto[2], Takayuki Yamamoto[2], Joonas A. Autio[1], Tomohisa Okada[2], Kaori Togashi[2], Hui Zhang[6], David C. Van Essen[3], Takuya Hayashi[1,7]

Affiliations:

[1]Laboratory for Brain Connectomics Imaging, RIKEN Center for Biosystems Dynamics Research, 6-7-3 Minatojima-minamimachi, Chuo-ku, Kobe 650-0047, Japan
Tel: 81-78-304-7140
Fax: 81-78-304-7141

[2]Department of Diagnostic Imaging and Nuclear Medicine, Kyoto University Graduate School of Medicine, Kawaramachi 54, Shogoin, Sakyo-ku, Kyoto city, 606-8507, Japan
Tel: 81-75-751-3111

[3]Department of Neuroscience, Washington University School of Medicine, Campus Box 8108, 660 South Euclid Avenue, St. Louis, MO 63110, USA
Tel: 314-362-3033

[4]Department of Radiology, Washington University School of Medicine, 660 S. Euclid Ave., St. Louis, MO 63110, USA
Tel: 314-362-7113

[5]Siemens Healthcare K.K., Gate City Osaki West Tower, 1-11-1, Osaki, Shinagawa-ku, Tokyo, 141-8644, Japan
Tel: 81-3-3493-7429

[6]Centre for Medical Image Computing and Department of Computer Science, University College London, The Front Engineering Building, Floor 3, Malet Place, London WC1E 7JE, UK
Tel: 44-20-7679-0320

bioRxiv preprint doi: https://doi.org/10.1101/441659; this version posted August 5, 2019. The copyright holder for this preprint (which was not certified by peer review) is the author/funder, who has granted bioRxiv a license to display the preprint in perpetuity. It is made available under aCC-BY-NC-ND 4.0 International license.

[7]RIKEN Compass to Healthy Life Research Complex Program, Integrated Innovation Building (IIB),
6-7-1 Minatojima-minamimachi, Chuo-ku, Kobe, Hyogo, Japan
Tel: 81-78-304-7140
Fax: 81-78-304-7141

Corresponding author
Takuya Hayashi, MD, PhD
Team Leader
Laboratory for Brain Connectomics Imaging
RIKEN Center for Biosystems Dynamics Research
6-7-3 Minatojima-minamimachi, Chuo-ku, Kobe 650-0047, Japan
Tel: 81-78-304-7140
Fax: 81-78-304-7141
E-mail: takuya.hayashi@riken.jp

Key words
neurite density, orientation dispersion, cortical mapping, diffusion tensor imaging, NODDI,

bioRxiv preprint doi: https://doi.org/10.1101/441659; this version posted August 5, 2019. The copyright holder for this preprint (which was not certified by peer review) is the author/funder, who has granted bioRxiv a license to display the preprint in perpetuity. It is made available under aCC-BY-NC-ND 4.0 International license.

Abstract

Diffusion tensor imaging (DTI) and neurite orientation dispersion and density imaging (NODDI) are widely used models to infer microstructural features in the brain from diffusion-weighted MRI. Several studies have recently applied both models to increase sensitivity to biological changes, however, it remains uncertain how these measures are associated. Here we show that cortical distributions of DTI and NODDI are associated depending on the choice of b-value, a factor reflecting strength of diffusion weighting gradient. We analyzed a combination of high, intermediate and low b-value data of multi-shell diffusion-weighted MRI (dMRI) in healthy 456 subjects of the Human Connectome Project using NODDI, DTI and a mathematical conversion from DTI to NODDI. Cortical distributions of DTI and DTI-derived NODDI metrics were remarkably associated with those in NODDI, particularly when applied highly diffusion-weighted data (b-value =3000 sec/mm^2). This was supported by simulation analysis, which revealed that DTI-derived parameters with lower b-value datasets suffered from errors due to heterogeneity of cerebrospinal fluid fraction and partial volume. These findings suggest that high b-value DTI redundantly parallels with NODDI-based cortical neurite measures, but the conventional low b-value DTI does not reasonably characterize cortical microarchitecture.

bioRxiv preprint doi: https://doi.org/10.1101/441659; this version posted August 5, 2019. The copyright holder for this preprint (which was not certified by peer review) is the author/funder, who has granted bioRxiv a license to display the preprint in perpetuity. It is made available under aCC-BY-NC-ND 4.0 International license.

1. Introduction

The diffusion motion of water molecules in brain tissue is affected by the local microarchitecture, including axons, dendrites and cell bodies. Diffusion tensor imaging (DTI) is a well-established model that describes Gaussian properties of diffusion motion in a fibrous structure like brain white matter from diffusion-weighted MRI (dMRI)[1,2], and is widely used for inferring the microstructural changes related to plasticity and diseases (for review, Johansen-Berg and Behrens, 2013)[3]. In most cases, summary parameters of DTI, fractional anisotropy (FA) and mean diffusivity (MD), have been studied based on dMRI data acquired with low b-value (b-value less than 1000), however, these parameters have not been shown to be specific to underlying microstructural features of axons and dendrites (collectively referred to as neurites) and are often sensitive to tissue compartments other than neurites[4].

One recent advance for estimating the microstructural complexity of brain tissue using dMRI is the Neurite Orientation Dispersion and Density Imaging (NODDI)[5]. NODDI models dMRI signals by combining three tissue compartments: neurites, extra-neurites, and cerebro-spinal fluid (CSF), each with different properties of diffusion motion, and enables in vivo estimation of a neurite density index (NDI) and an orientation dispersion index (ODI), as well as a volume fraction of isotropic diffusion (V_{iso}). NODDI requires dMRI data to be scanned with multiple b-values (e.g. b=700 and 2000 sec/mm^2) and relatively higher number of diffusion gradient directions (e.g. >90 directions over two b-shell) as compared with DTI[5]. The NDI estimates the volume fraction of neurites, including both axons and dendrites, whereas the ODI estimates the variability of neurite orientation: ranging from 0 (all parallel) to 1 (isotropically randomly oriented). NODDI has already been applied to many studies because of their feasibility. The variation of NODDI estimates in white matter have been related to aging[6–11] and neurologic disorders[12–14]. Of note, NODDI has proven to be useful for gray matter neurite changes as reported in several clinical studies, e.g. in patients with IFN-α-induced fatigue[15], Wilson's disease[16], cortical dysplasia[17], aging[18], and schizophrenia[19]. We recently optimized NODDI for cortical gray matter[20], finding that the NODDI reflects neurobiology of cortical microarchitecture – cortical distribution of NDI is closely related to cortical myelin[21] and ODI is associated with cortical organization of radial/horizontal fibers[22,23]. Although there is recent debate about oversimplified assumptions in NODDI such as uniform diffusivity[24], it is of note that accumulated histological evidence indicates that NDI and ODI of neural tissues are reasonably representing histology-based neurite density[25] and orientation dispersion[25–28], respectively.

Recently, there is accumulating evidence of combined DTI and NODDI analysis in clinical studies.

bioRxiv preprint doi: https://doi.org/10.1101/441659; this version posted August 5, 2019. The copyright holder for this preprint (which was not certified by peer review) is the author/funder, who has granted bioRxiv a license to display the preprint in perpetuity. It is made available under aCC-BY-NC-ND 4.0 International license.

Those performed both DTI and NODDI in the pathological cortex all showed opposite changes between MD and NDI in Parkinson's disease[29], multiple sclerosis[25], and stroke[30]. Our previous study also revealed that strong relationships between NODDI and DTI parameters in the cortex of healthy subjects, in particular, NDI and 1/MD were very highly correlated (R=0.97)[20] when used three-shell dMRI data including high b-value, but not so highly correlated when used low b-value data. On the other hand, in vitro study showed that slower-decaying component found by high b-value dMRI signals were originated from intra-neurite water[31], thus suggesting that MD obtained at high b-value is specifically reflecting neurite properties. High b-value DTI in clinical studies also implicate higher sensitivity to neurobiological changes than low b-value, e.g. the contrast between gray/white matter[32], ischemic/hypoxic changes in the gray matter[33], white matter disintegrity in schizophrenia[34] and maturation in juveniles[35]. However, there is no consensus how DTI is associated with NODDI parameters, and how it is dependent on the b-shell scheme.

In this study, we investigated how DTI and NODDI parameters are related with each other in cortical gray matter in healthy subjects. The measures were correlated by two methods and also analyzed by utilizing a recently derived mathematical function, which converts DTI to NODDI parameters[24,36]. We used the preprocessed dMRI data from Human Connectome Project (HCP), and estimated b-shell scheme dependency of the relationship between DTI and NODDI parameters. Since the function relies on the assumption that CSF compartment (V_{iso}) is negligible in the tissue[24,36], we also estimated V_{iso} in the cortex and the white matter based on previous work[20] and estimated effect on the partial voluming and the relationship between DTI and NODDI parameters. We performed simulation analysis in terms of b-value, proportion of CSF signal. Our main purpose is to highlight the neurite properties in the specific subtype of brain, cortical gray matter, in healthy subjects, and investigate how DTI specifically represent the cortical NODDI metrics. We also review the past literature which applied NODDI and DTI in vitro and in vivo dMRI studies and discuss the potential interpretability of DTI.

2. Materials and Methods

In order to comprehensively investigate the relationship between NODDI and DTI in cortical gray matter, we examined whether NODDI parameters can be accurately estimated from DTI using their mathematical relation. Publicly available MRI data from 456 healthy subjects (aged 22-35 years) the HCP (https://www.humanconnectome.org/) were used. In particular, dMRI datasets with different b-shell structures were analyzed to investigate how the b-shell scheme affects the relationship between two diffusion model. To clarify why their relationship depends on the diffusion scheme, we

bioRxiv preprint doi: https://doi.org/10.1101/441659; this version posted August 5, 2019. The copyright holder for this preprint (which was not certified by peer review) is the author/funder, who has granted bioRxiv a license to display the preprint in perpetuity. It is made available under aCC-BY-NC-ND 4.0 International license.

also performed simulation analysis addressing several error sources such as CSF signals in dMRI data and partial volume effects. Data analyses were performed at RIKEN, and the use of HCP data in this study was approved by the institutional ethical committee (KOBE-IRB-16-24).

2.1.1 *Subjects and dMRI datasets*

We used the 'S500 Release Subjects' dataset from the publicly available HCP dataset, including high-resolution structural images (0.7-mm isotropic T1w and T2w images,[37] and dMRI data (1.25-mm isotropic resolution)[38]. The dMRI data obtained with TR=5520ms and TE=89.5ms included 270 volumes with 90 volumes for each of the three shells of b-values (b=1000, 2000 and 3000 s/mm^2) in addition to 18 non-diffusion weighted (b=0 s/mm^2) volumes. From this dataset, 456 healthy subjects (age, 22-35 years) scanned with a complete dataset of 270 volumes were chosen, and 49 subjects were excluded based on incomplete dMRI scans. In our previous study, NDI and the reciprocal of MD (1/MD) showed very similar surface distributions when all of the dMRI data were used, but they did not show similar distributions when only a single shell of b=1000 dMRI data was used[20]. Therefore, we hypothesized that the relationship between DTI and NODDI may differ depending on the b-shell scheme of dMRI data. To address this, datasets with different b-shell schemes were used for analysis (Table 1), i.e. for each subject, seven types of b-shell datasets were derived from dMRI data as follows: three one-shell datasets using b=0 volume and any one of b=1000, 2000, or 3000 volume; three two-shell datasets using b=0 images and any two of b=1000, 2000, or 3000 volume; and a three-shell dataset using all images.

2.1.2 *Calculation of the cortical surface map of original NODDI and DTI-derived NODDI parameters*

The DTI estimates (FA and MD) were calculated using each dataset of dMRI and the dtifit diffusion tensor modeling tool in Functional Magnetic Resonance Imaging of the Brain Software Library (FSL) 5.09 (http:// www.fmrib.ox.ac.uk/fsl). This linear DTI model was applied not only to a single-shell 'standard' b=1000 data but also to high b-value and multi-shell dMRI datasets. The primary reason of 'forced' fitting of DTI to such data was that we unexpectedly found correspondence of DTI metrics with those of NODDI in our previous paper. While it is known that these high b-value/multi-shell data take non-Gaussian distribution thus are more appropriate to apply a non-linear model like diffusion kurtosis imaging (DKI)[39], there have been also a few reports that high b-value DTI sensitively detect the brain tissue pathologies[32–35]. The diffusion data were also fitted to the NODDI model using the optimized value of $d_{//}$ and Accelerated Microstructure Imaging via Convex Optimization (AMICO) 1.0[40], which re-formulates the original NODDI model as a linear

bioRxiv preprint doi: https://doi.org/10.1101/441659; this version posted August 5, 2019. The copyright holder for this preprint (which was not certified by peer review) is the author/funder, who has granted bioRxiv a license to display the preprint in perpetuity. It is made available under aCC-BY-NC-ND 4.0 International license.

system and shortens the calculation time. The value of $d_{//}$ was optimized for the cerebral cortex (1.1×10^{-3} mm^2/s) and changed from the default value (1.7×10^{-3} mm^2/s)[20], because we are interested in the cerebral cortical gray matter. We used default values of regularization (λ=0.001 and γ=0.5) for AMICO.

The parameters of the original NODDI model (NDI_{ORIG} and κ) and the DTI model (FA and MD) were mapped onto the cortical surface, as described previously[20]. Briefly, the algorithm for surface mapping identifies cortical ribbon voxels within a cylinder orthogonal to the local surface for each mid-thickness surface vertex on the native mesh and weights them using a Gaussian function (FWHM= ~4 mm, σ=5/3 mm), which reduces the contribution of voxels that contain substantial partial volumes of CSF or white matter[21]. The ODI in the original NODDI (ODI_{ORIG}) was calculated using the surface metric of κ and equation (5). The maps of DTI-derived NODDI parameters (NDI_{DTI} and ODI_{DTI}) were calculated by converting from DTI maps to NODDI maps based on the mathematical relation (Fig. 1 and Supplementary text 1.2). The surface maps were resampled using MSMAll surface registration[41–43] and onto the 32k group average surface mesh. For surface-based analysis, we used Connectome Workbench (https://github.com/Washington-University/workbench, Marcus et al., 2013). The scripts used in this manuscript are available from NoddiSurfaceMapping (https://github.com/RIKEN-BCIL/NoddiSurfaceMapping).

2.1.3 *Statistical analysis*

Surface maps of NDI_{ORIG}, ODI_{ORIG}, V_{iso}, NDI_{DTI} and ODI_{DTI} using each dataset were averaged across subjects and parcellated using the HCP's multi-modal cortical parcellation (HCP_MMP1.0 210P MPM version)[41]. The mean value of each measure for each of the 180 parcels per hemisphere was calculated. NDI_{ORIG} and ODI_{ORIG} calculated using all the dMRI data were considered 'a gold standard' reference. To investigate the linear relationship between DTI-derived NODDI parameters and the original NODDI parameters, the correlations between each parcellated surface map (NDI_{ORIG}, ODI_{ORIG}, NDI_{DTI} and ODI_{DTI}) and the reference in each subject were calculated using Pearson correlation analysis. To investigate whether DTI-derived NODDI parameters are biased, Bland-Altman analysis was performed in each dataset[45]. Briefly, Bland-Altman analysis is a method to confirm the presence or absence and degree of systematic bias visually by creating a scatter diagram (Bland-Altman plot), which is created by plotting the difference between two pairs of measured values on the y axis and the average value of the two measured values on the x axis.

Since the quality of the NODDI estimates depends on the image quality and preprocessing, we

bioRxiv preprint doi: https://doi.org/10.1101/441659; this version posted August 5, 2019. The copyright holder for this preprint (which was not certified by peer review) is the author/funder, who has granted bioRxiv a license to display the preprint in perpetuity. It is made available under aCC-BY-NC-ND 4.0 International license.

estimated the practical quality by the temporal signal-to-noise ratio (tSNR) of preprocessed b=0 volumes and removed 29 surface parcels with tSNR<17 from the analysis. Therefore, a total of 331 parcels in the whole cortex were used for the analysis. The cutoff was determined empirically in our previous study[20].

2.2 *Simulation for the effect of heterogeneity in CSF volume fraction on parameters of NODDI, DTI and DTI-derived NODDI*

Since correlations and biases between original NODDI and DTI-derived parameters were dependent on the presence of high b-value data (b=3000 s/mm^2) in the datasets (see section 3.1), simulations were performed to clarify whether and how potential sources of error can explain our findings of cortical DTI-derived parameters. One of potential sources is the amount of CSF compartment (V_{iso}) in the voxel, which may be sum of intra-tissue CSF volume and partial voluming of CSF in the subarachnoid space (see also Supplementary text 2, Fig. S1). This compartment is not considered in the DTI or assumed to be zero in the DTI-derived NODDI calculation. The various levels or 'heterogeneity' of CSF volume fraction in the cortical voxel can cause errors at various level and could result in biases of the cortical distribution. Although actual heterogeneity of CSF volume fraction in the cortex cannot be measured in vivo, the simulation for the error sensitivity of diffusion measures to varying level of CSF volume fraction may give some insights. Another source of the error may be an interaction between heterogeneity CSF volume fraction and b-shell scheme of the data, since low b-value dMRI data may contain more CSF signal than high b-value dMRI data. Therefore, we tested how variable level of CSF and b-shell scheme can cause changes in the parameters of the original NODDI, DTI and DTI-derived NODDI in comparison with those calculated in reference condition of NDI=0.25, ODI=0.30 and V_{iso}=0.1, the mean value of cortex[20]. The values of V_{iso} were varied from 0 to 0.6 (i.e. ΔV_{iso} from -0.1 to 0.5 in reference to V_{iso}=0.1) with an interval of 0.1. Parameters of NODDI was calculated using the simulated three-shell dataset (b_{All}) and those of DTI and DTI-derived NODDI was calculated using any of seven b-shell datasets (Table 1). The simulation data was created based on the mathematical equations and derivation described in the Supplementary text 3.1. To confirm the specificity of this findings, we also performed another simulation in which 'homogeneous' but small CSF volume fraction was assumed (Supplementary Text 3.2). The bias of DTI-derived NODDI and DTI parameters were also assessed by Bland-Altman analysis. (Supplementary text 3.2).

3. Results

3.1 Cortical maps of DTI-derived NODDI parameters using in vivo dMRI data

bioRxiv preprint doi: https://doi.org/10.1101/441659; this version posted August 5, 2019. The copyright holder for this preprint (which was not certified by peer review) is the author/funder, who has granted bioRxiv a license to display the preprint in perpetuity. It is made available under aCC-BY-NC-ND 4.0 International license.

When the three-shell dataset (b_{All}) in 456 subjects of HCP data were used in the original NODDI, the cortical map of neurite density (NDI_{ORIG}) showed high intensity in the primary sensorimotor, visual, auditory cortices as well as the middle temporal (MT) area (Fig. 2A), while ODI_{ORIG} showed high intensity in the primary sensory, visual and auditory areas (Fig. 3A), as we reported previously[20]. Moreover, consistent with our previous study[20], the cortical distribution of the NDI_{ORIG} was quite similar to that of the myelin map based on the T1w and T2w images, while the distribution of ODI_{ORIG} showed high contrast in the 'granular cortex' of von Economo and Koskinas [23], where cortical thickness is low and both radial and horizontal fibers are intermingled[20].

When using same three-shell dataset (b_{All}), cortical distribution of MD showed extremely inversed appearance to NDI_{ORIG} (Fig. 2B) as reported previously[20] — this was also true when using high b-value one-shell dataset (b_{3000}) (Fig. 2E), but not when using low b-value one-shell dataset (b_{1000}) (Fig. 2H). In correlation analysis using the parcellated data (see Methods & Materials 2.1.3), MD strongly negatively correlated with NDI_{ORIG} when using three-shell dataset (b_{All}) ($R=-0.96$, $p<0.00001$) and high b-value one shell (b_{3000}) ($R=-0.86$, $p<0.00001$), but did not strongly correlate when using low b-value one-shell dataset (b_{1000}) ($R=-0.31$, $p<0.00001$) (Fig. 4). As for FA, cortical maps of FA showed moderate inversed appearance to ODI_{ORIG} and (negative) correlation with ODI_{ORIG} among all datasets ($R=-0.40 \sim -0.62$) (Fig. 3, 4). There were not strong correlations between FA and NDI_{ORIG} in any b-shell dataset ($R=0.15 \sim 0.28$) (Fig. 4).

DTI-derived NODDI maps (NDI_{DTI}, ODI_{DTI}) also showed very similar cortical distributions of NDI and ODI in average surface maps across all subjects (Fig. 2A, C, F for NDI_{DTI} and Fig. 3A, C, F for ODI_{DTI}), particularly when using high b-value dataset including b_{All} and b_{3000}. The correlation analysis showed that correlation coefficients between the DTI-derived NODDI and original NODDI parameters were extremely high for both NDI (NDI_{DTI}/b_{All}: $R=0.97$, NDI_{DTI}/b_{3000}: $R=0.87$, $p<0.00001$) and ODI (ODI_{DTI}/b_{All} $R=0.94$, ODI_{DTI}/b_{3000} $R=0.86$, $p<0.00001$) (Fig. 4).

To investigate the agreement of DTI-derived NODDI compared with the original NODDI, the Bland-Altman analysis was applied to the values of cortical parcellations using those of complete data and original NODDI as a reference. When all of the dMRI data (b_{All}) were used, the results of DTI-derived NODDI showed a consistent bias: NDI_{DTI} overestimated by a difference of around 0.20 and ODI_{DTI} by 0.15 to 0.10 as compared with those of original NODDI (Fig. 5 A, C). The $NDI_{DTI}/b_{3000,}$ (Fig. 5B) also showed a consistent bias, which was a little smaller than NDI_{DTI}/b_{All} (Fig. 5A). The bias of ODI_{DTI}/b_{3000} (Fig. 5D) was almost same as in the three-shell dataset (Fig. 5C).

bioRxiv preprint doi: https://doi.org/10.1101/441659; this version posted August 5, 2019. The copyright holder for this preprint (which was not certified by peer review) is the author/funder, who has granted bioRxiv a license to display the preprint in perpetuity. It is made available under aCC-BY-NC-ND 4.0 International license.

Other datasets including a high b-value shell also provided comparable results with the original NODDI (Fig. S3-4). If b=3000 is included in the two-shell data ($b_{1000\text{-}3000}$ and $b_{2000\text{-}3000}$), both NDI_{DTI} and ODI_{DTI} showed a similar surface distribution to the reference (Fig. S3 A, D, F, Fig. S4 A, D, F). The correlation coefficients were very high in the group-wise maps for both NDI_{DTI} and ODI_{DTI} ($b_{1000\text{-}3000}$: R=0.97, R=0.89, $b_{2000\text{-}3000}$: R=0.93, R=0.92, respectively, $p<0.00001$) (Fig. 4). The Bland-Altman analysis showed that the dataset of high and low b-value two-shell ($b_{1000\text{-}3000}$) (Fig. S5) had a constant bias of NDI_{DTI} and slightly upward sloping bias of ODI_{DTI}, which were almost the same size as in the three-shell dataset. High b-value two-shell ($b_{2000\text{-}3000}$) (Fig. S5 A) had also a constant bias of NDI_{DTI} but with a somewhat smaller size than that in three-shell dataset (b_{All}). The bias of ODI_{DTI} was almost same size as in the three-shell dataset (Fig. 5 C, S5 B).

The dataset not including a high b-value shell showed inconsistent cortical distributions with the reference. For the two-shell dataset ($b_{1000\text{-}2000}$), NDI_{DTI} was a little different and the correlation coefficient was moderate (R=0.71, $p<0.00001$) (Fig. 4), while ODI_{DTI} showed relatively high correlations in the group-wise maps (R=0.84, $p<0.00001$) (Fig. 4). One-shell datasets using lower b-value shells (i.e. b_{1000} and b_{2000}) did not provide comparable surface maps of NDI_{DTI} (Fig. S3 L, N) and ODI_{DTI} (Fig. S4 L, N). For example, for the low b-value one-shell dataset (b_{1000}), both NDI_{DTI} and ODI_{DTI} showed different surface distributions from the reference (Fig. S3 A, N, Fig. S4 A, N), as well as very low correlation coefficients for NDI_{DTI} (R=0.33 $p<0.00001$) and ODI_{DTI} (R=0.58, $p<0.00001$) (Fig. 4). This trend was also found when using the middle high b-value one-shell dataset (b_{2000}). Only ODI_{DTI} showed a similar surface distribution to the reference (Fig. S4 A, L) and high correlation coefficients (R=0.80, $p<0.00001$) (Fig. 4), while NDI_{DTI} showed different surface distribution from the reference (Fig. S3 A, L) and relatively low correlations (R=0.59, $p<0.00001$) (Fig. 4).

When comparing original NODDI parameters using one- or two-shell datasets to the reference, any two-shell datasets provided similar surface maps of NDI_{ORIG} and ODI_{ORIG} with the reference and they were highly correlated (R>0.91, $p<0.00001$) (Fig. S6). However, NDI_{ORIG} using low b-value one-shell datasets were not significantly correlated to the reference (R<0.19, $p>0.00001$), while ODI_{ORIG} was relatively correlated even though using one-shell datasets (R>0.71, $p<0.00001$) (Fig. S6), as show in the simulation study in Zhang et al[5].

3.2 *Simulation for the effect of heterogeneity in CSF volume fraction on parameters of NODDI, DTI*

bioRxiv preprint doi: https://doi.org/10.1101/441659; this version posted August 5, 2019. The copyright holder for this preprint (which was not certified by peer review) is the author/funder, who has granted bioRxiv a license to display the preprint in perpetuity. It is made available under aCC-BY-NC-ND 4.0 International license.

and DTI-derived NODDI

We simulated the percent changes in NODDI, DTI and DTI-derived NODDI depending on altered CSF compartment (V_{iso}) and b-shell dataset. As compared with the reference condition (V_{iso}=0.1), apparent differences in amount of change in the parameters were found across type of calculation (NODDI, DTI, DTI-derived NODDI) and b-shell schemes (Fig. 6). While the original NODDI using all the b-shell dataset (b_{All}) was reasonably unbiased by altered V_{iso}, the parameters of DTI and DTI-derived NODDI tended to be largely biased particularly used b-shell datasets not including high b-value volumes (b=3000) (b_{1000}, b_{2000}, and $b_{1000\text{-}2000}$) (Fig. 6). The dataset including high b-value (b_{3000}, $b_{1000\text{-}3000}$, $b_{2000\text{-}3000}$ and b_{All}) were relatively less biased across ranges of V_{iso} changes. These findings suggest that the error of DTI derived parameters is sensitive to the heterogeneity of CSF partial voluming, particularly when lower b-value data was applied. To confirm the specificity of this findings, we also performed another simulation in which 'homogeneous' but small CSF volume fraction was assumed (Supplementary Text 3.2). This confirmed that correlation between original NODDI and DTI-derived NODDI was reasonably high as long as CSF volume fraction is not 'heterogeneous'.

Discussion

Accumulating evidence have suggested that high b-value dMRI signal is more sensitive to neurites and neural tissue changes than low b-value dMRI signal. The in vitro study of optic nerve with q-space analysis of diffusion-weighted spectroscopy[31] identified slower-decaying component of dMRI signals which have 1) diffusion displacement restricted to ~2 μm close to axonal diameter, 2) longer T2 than rapid diffusing components including myelin water and 3) dependency on neurite orientation, thus suggesting that this component originated from intra-neurite water. The T2 time for myelin water is very short (10-20ms), while intra- and extra-cellular water is longer than 60ms[46], thus making dMRI signals with TE=89.5ms insensitive to myelin water. The dependency of high b-value diffusion-weighted signal on neurite orientation is largely caused by neurite membrane rather than by other longitudinal structures including myelin and neurofilaments[47]. Simulation showed that the majority of dMRI signals with b-value less than 1000 s/m^{-2} represents fast-diffusion components which may originate free water such as in CSF compartment. On the other hand, recent high b-value DTI in clinical studies showed higher sensitivity to neurobiological changes than low b-value — apparent diffusion coefficient from high b-value DTI was sensitive to the contrast between gray/white matter[32], ischemic/hypoxic changes in the gray matter[33], white matter disintegrity in schizophrenia[34] and maturation in juveniles[35]. Taken together, signals obtained at high b-value are likely sensitive to neurobiological changes including neurites, however, there is not

bioRxiv preprint doi: https://doi.org/10.1101/441659; this version posted August 5, 2019. The copyright holder for this preprint (which was not certified by peer review) is the author/funder, who has granted bioRxiv a license to display the preprint in perpetuity. It is made available under aCC-BY-NC-ND 4.0 International license.

completely established model that quantitates a specific property of neurites. The DTI and NODDI are among the most widely used models: the former is a simplified linear model that accounts for Gaussian process of diffusion motion of water molecule in the tissue, and the latter explicitly models neurite properties in the tissue based on non-linear nature in high b-value data.

The NODDI is among the most validated models for its predictability of neurite properties. Accumulated histological evidence indicates that NDI and ODI of brain and spinal cord tissues are reasonably correlated with histology-based neurite density[25] and orientation dispersion[25–28], respectively. The NODDI ODI is relatively robust against data quality[5], and well represented the histology-based neurite orientation dispersion in all the studies[25–28] including a single shell and multi-shell dMRI. It is notable that by applying multi-shell dMRI in the spinal cord specimen of multiple sclerosis. Grussu et al. [25] revealed that NDI of NODDI was fairly correlated with histology-based density of neurites as assessed by staining neurofilaments. However, since the intrinsic diffusivity is simplified[5] (see section of Limitation), careful attention is needed for potential bias depending on the diffusivity, for example, when mixing analysis across tissue subtypes such as gray and white matter[20]. Therefore, we estimated specific tissue subtype, cortical gray matter and analyzed the relation of DTI metrics, DTI-derived NODDI metrics to the original NODDI.

Here, we showed in healthy subjects that cortical metrics of DTI and DTI-derived NODDI parameters were highly correlated with those of original NODDI, when used a particular set of b-shell scheme in dMRI. 1) the DTI MD was negatively correlated with NODDI NDI when data included high b-value (b=3000) (R>0.9), 2) the DTI FA was partially correlated with NODDI ODI and NDI particularly when used middle to lower ranged b-value (b=1000-2000) (R>0.87), 3) both NDI and ODI of DTI-derived NODDI showed high correlation with the original NODDI (R>0.9) when used dMRI data including high b-value (b=3000). Simulation analysis suggests that less relation of DTI to NODDI when used low b-value data is due to higher sensitivity to heterogeneity in CSF volume fraction in the intra-tissue and/or partial volume. The HCP data and simulation showed that high b-value dMRI data resulted in a constant numerical bias, i.e. same amount of error over the range of values, potentially due to the bias in the DTI measures coming from non-Gaussian distribution of high b-value dMRI data. Since high b-value dMRI data is often in non-Gaussian distribution, applying linear DTI model for such high b-value dMRI data may result in biases of calculated measures as compared with those used b=1000 dMRI data. Past literature also notes that when using high b-value dMRI data, the values of MD were underestimated[48] and those of FA were overestimated[4,49,50] compared with those of b=1000 dMRI data. We've also confirmed in the

bioRxiv preprint doi: https://doi.org/10.1101/441659; this version posted August 5, 2019. The copyright holder for this preprint (which was not certified by peer review) is the author/funder, who has granted bioRxiv a license to display the preprint in perpetuity. It is made available under aCC-BY-NC-ND 4.0 International license.

simulation that the biases are constant over a possible range of values between DTI-derived NODDI and original NODDI (data not shown). Therefore, the bias of DTI may be due to the effect of kurtosis of high b-value dMRI data. These findings indicate that DTI parameters in cortical gray matter are highly related to those of NODDI when analyzed using high b-value dMRI data and are not very predictive when used low b-value dMRI. This suggests that analyzing cortical microarchitecture by both DTI and NODDI is redundant and does not surpass usefulness of cortical neurite mapping by either way.

The DTI and DTI-derived NODDI were sensitive to the errors caused by heterogeneity of CSF volume fraction and b-shell scheme of the data. When not using the high b-value shell, the cortical distribution of DTI-derived NODDI parameters showed completely different pattern from those of original NODDI (Fig. S3-4). Our simulation suggests this is because low b-value DTI-derived NODDI parameters are more sensitive to change in V_{iso} due to heterogeneity and partial voluming of CSF (Fig. 6). Low b-value dMRI is theoretically sensitive to fluid signals or 'T2 shine-through' effect as well as to tissue diffusivity, whereas high b-value dMRI is more specific to tissue diffusivity[32,51]. In addition, the partial volume effects of CSF may vary across cortical regions according to cortical thickness and their heterogeneity within the cortex. The effect is not completely removed even though the partial volume effect is reasonably reduced by surface-based analysis as compared with volume-based analysis (see Supplementary text 2, Fig. S1). Moreover, the model of DTI by itself does not account for multi compartments in the tissue and also suffers from a partial volume effect of CSF and results in fitting error particularly in the cortex[2,52]. In contrast, the NODDI explicitly considers a CSF compartment s is insensitive to the heterogeneity of CSF as shown in the simulation study (Fig 6). The high b-value DTI and DTI-derived NODDI parameters were also biased in a fixed manner (Fig 5 and Supplementary text 3.2), which are likely caused by non-Gaussian distribution[36]. The values of MD were underestimated and those of FA were overestimated (Supplementary Text 3.2) in high b-value datasets, consistent with previous studies for MD[48] and FA[4,49,50].

The current study gives insights and interpretations into recent studies which applied NODDI and DTI in the same sample. In particular, NODDI and DTI showed different sensitivity to the neurobiological changes of interest, while there is a potential variety of CSF contamination and data sampling. Grussu et al. studied NODDI and DTI in spinal cord in healthy subjects[53]. They applied DTI to low b-value dMRI and NODDI to multi-shell data and found that NODDI ODI was the most sensitive to the contrast between gray and white matter. Kamagata et al., applied both DTI and

bioRxiv preprint doi: https://doi.org/10.1101/441659; this version posted August 5, 2019. The copyright holder for this preprint (which was not certified by peer review) is the author/funder, who has granted bioRxiv a license to display the preprint in perpetuity. It is made available under aCC-BY-NC-ND 4.0 International license.

NODDI parameters in Parkinson's disease and controls using multi-shell dMRI data[29]. The DTI was calculated using low b-value data (b=1000) and NODDI with 2-shell of b=1000 and 2000. Interestingly, both NDI and ODI of the NODDI metrics in the cortical gray matter were more sensitive to discriminate patients from controls than those of DTI, which may support higher sensitivity of NODDI than low b-value DTI to the neuropathological changes in this disease. These are in line with our result that DTI-derived NODDI parameters with low to middle b-value data was not strongly correlated with the high b-value NODDI parameters. Mah et al. also studied NODDI and DTI in early adolescent brain and found that NODDI NDI was more sensitive to age-related changes as compared to DTI MD[54]. They also showed that subcortical gray matter structures, which may be less affected by partial voluming CSF than cortex, showed high correlation between MD and NDI (R=0.69-0.88) and between FA and ODI (R=0.70-0.81). In addition, Batalle et al. analyzed cortical metrics of NODDI and DTI in infant brain and results were complicated[55]. They applied relatively low-resolution dMRI (2mm) for small sized brain and found the dissociated pattern of changes in the cortical NDI and MD. As expected, MD and NDI showed inversed pattern across ages but only after gestational age of 38-week. Parallel pattern between MD and NDI was found before age of 38-week, which may be due to errors in partial voluming of CSF due to small sized brain and thin cortex. The partial volume effect of CSF may not be negligible in their results, since DTI data was calculated based on the low b-value dMRI data.

Preclinical studies also showed neurobiological changes by NODDI and DTI. Using Alzheimer's model of transgenic mice, Colgan et al. performed NODDI and DTI using multi-shell dMRI data and found higher sensitivity of NODDI NDI than low b-value DTI MD to histology-based marker of neurodegeneration, tau immunoreactivity[56]. The in vitro study using spinal cord specimen of multiple sclerosis was scanned with multi-shell dMRI including high b-value. They also showed that MD of DTI was negatively correlated with histology-based neurite density in the same specimen. Our previous study which used multi-shell dMRI data also found a very strong relationship between DTI MD and NODDI NDI and that values of FA was also associated with ODI depending on the MD[20].

This study provides important implications for future dMRI studies. First, it is redundant to apply both DTI and NODDI to dMRI data for estimating microstructure in cortical gray matter. As formulated by a mathematical conversion from DTI to NODDI, there is no additional quantitative information available by applying both. When used low b-value dataset, DTI suffers from the errors of CSF heterogeneity as compared with NODDI. Therefore, users can choose either method

bioRxiv preprint doi: https://doi.org/10.1101/441659; this version posted August 5, 2019. The copyright holder for this preprint (which was not certified by peer review) is the author/funder, who has granted bioRxiv a license to display the preprint in perpetuity. It is made available under aCC-BY-NC-ND 4.0 International license.

depending on the dMRI data acquired, and neurobiological significance may not be changed. Second, a high b-value DTI is potentially useful for cortical neurite mapping, particularly in clinical setting. A shorter dMRI scan will be particularly helpful for clinical patients such as patients with Alzheimer's disease who cannot keep still long time. DTI can be estimated with relatively few directions - at least 6 or in general more than 30 are recommended [57], whereas the original NODDI is recommended with at least 90 directions [5], which means three times higher efficiency. HCP-style scanning with high spatial resolution dMRI with 30 directions does not exceed 3 min. Third, low b-value DTI is not appropriate for cortical mapping and suffer from errors from heterogeneity and partial voluming of CSF. The heterogeneity itself cannot be completely estimated by the currently available resolution of dMRI. A special sequence, such as 'fluid-attenuated inversed recovery DTI', can be useful by reducing CSF signals [58,59]. Meanwhile, the NODDI is more robust against the errors from CSF partial voluming for cortical mapping of microarchitecture.

One of limitations of this study is that it relies on the relative validity of NODDI over DTI. Recently, there is subject of debate about the eligibility on simplification in the NODDI associated with constrained intrinsic diffusivity[24,60]. There is an attempt to develop a novel method that explicitly analyzes local complexities of diffusivity[24]. The method is potentially useful for future application; however, it is technically demanding for scanning, particularly, specific diffusion gradient encoding both in linear tensor and spherical tensor. There is also need for investigations on whether the intrinsic diffusivity is significantly changed in-vivo and how it influences the quantification of neurite properties in the gray matter. In the previous study, we optimized the intrinsic diffusivity for the gray matter (1.1×10^{-3} mm^2/s) based on non-linear multiparametric fitting[20], which resulted in reasonable findings of correlation between neurite density and myelin contrast as expected from histological evidence[61,62]. Second, we did not analyze the relationship between DTI and NODDI in the 'white matter' in this article. We estimated that the volume fraction of isotropic diffusion is larger in the white matter (0.21±0.1) than in the gray matter (0.09±0.06) (see also Supplementary Text 2), as expected from the fact that the white matter is also a major site for convective flow of CSF[63]. Despite potential larger fraction of CSF, the white matter is not affected by partial voluming of CSF in the subarachnoid space like in the cortical gray matter. Therefore, as long as the volume fraction of CSF is relatively heterogenous across regions in the white matter, the relationship of NODDI and DTI may be similar to those in the gray matter. This is also supported by the current simulation studies on heterogeneity of CSF volume fraction as shown in section 3.2 and

bioRxiv preprint doi: https://doi.org/10.1101/441659; this version posted August 5, 2019. The copyright holder for this preprint (which was not certified by peer review) is the author/funder, who has granted bioRxiv a license to display the preprint in perpetuity. It is made available under aCC-BY-NC-ND 4.0 International license.

Supplementary Text 3.2. Third, we applied DTI model for multi-shell dMRI datasets, which are known to have non-Gaussian distribution. Mathematically, non-linear model like DKI[39] is more suitable for such non-Gaussian dMRI data than DTI. There is also evidence that parameters of DTI such as FA and MD are comparable with those from DKI[64], however, we did not include the comparison of DKI with NODDI in this study because of limited space.

5. Conclusion

For addressing cortical microarchitecture, conventional DTI with low b-value dataset is not very useful because of contamination with the heterogeneity of CSF, whereas NODDI is robust against these factors. Cortical DTI parameters were closely associated with those of NODDI, particularly using data including high b-value data. DTI-derived NODDI based on high b-value dataset showed remarkably similar cortical distributions with those of NODDI, supporting the previous notion of the mathematical conversion between the DTI and NODDI. Simulation also supported these findings that potential intra-tissue CSF fraction and partial voluming of arachnoid CSF may be causing the error and bias in the cortical maps different from those of original NODDI. Although its similarity, analyzing with high b-value dataset and DTI does not add more information for cortical microarchitecture than NODDI.

6. Notes

Data of figures and supplementary figures are available at https://balsa.wustl.edu/study/show/G331M

7.Ethics Statement

The use of HCP data in this study was approved by the institutional ethical committee (KOBE-IRB-16-24).

8. Author Contributions

HF and TH designed the study. HF, KM and TH made programs for analysis. HF, TH, TA, KF, TY, TO, and KT analyzed the data. HF, TH, MG, HZ, JA, and DV contributed to writing the manuscript. All authors have read and approved the final manuscript.

9. Conflict of Interest Statement

Author Katsutoshi Murata was employed by company Siemens Healthcare K.K. Japan, and contributed to analysis, while the present study was not financially supported by Siemens Healthcare K.K. Japan. All other authors declare no competing interests.

bioRxiv preprint doi: https://doi.org/10.1101/441659; this version posted August 5, 2019. The copyright holder for this preprint (which was not certified by peer review) is the author/funder, who has granted bioRxiv a license to display the preprint in perpetuity. It is made available under aCC-BY-NC-ND 4.0 International license.

10. Acknowledgements

The data of this study were provided by the Human Connectome Project, WU-Minn Consortium (Principal Investigators: David Van Essen and Kamil Ugurbil; 1U54MH091657) funded by the 16 NIH Institutes and Centers that support the NIH Blueprint for Neuroscience Research; and by the McDonnell Center for Systems Neuroscience at Washington University. This research is partially supported by the program for Brain Mapping by Integrated Neurotechnologies for Disease Studies (Brain/MINDS) and Brain/MINDS-beyond from Japan Agency for Medical Research and development, AMED (JP18dm0207001, JP19dm0307006h0002), by RIKEN Compass to Healthy Life Research Complex Program from Japan Science and Technology Agency, JST, by MEXT KAKENHI Grant (16H03300, 16H03306) (T.H.).

bioRxiv preprint doi: https://doi.org/10.1101/441659; this version posted August 5, 2019. The copyright holder for this preprint (which was not certified by peer review) is the author/funder, who has granted bioRxiv a license to display the preprint in perpetuity. It is made available under aCC-BY-NC-ND 4.0 International license.

References

1. Basser, P. J., Mattiello, J. & Lebihan, D. Estimation of the Effective Self-Diffusion Tensor from the NMR Spin Echo. *J. Magn. Reson. B* **103**, 247–254 (1994).
2. Basser, P. J., Mattiello, J. & LeBihan, D. MR diffusion tensor spectroscopy and imaging. *Biophys. J.* **66**, 259–267 (1994).
3. Johansen-Berg, H. & Behrens, T. Diffusion MRI: From Quantitative Measurement to In vivo Neuroanatomy: Second Edition. 1–614 (2013).
4. Pierpaoli, C. & Basser, P. J. Toward a quantitative assessment of diffusion anisotropy. *Magn. Reson. Med.* **36**, 893–906 (1996).
5. Zhang, H., Schneider, T., Wheeler-Kingshott, C. A. & Alexander, D. C. NODDI: Practical in vivo neurite orientation dispersion and density imaging of the human brain. *NeuroImage* **61**, 1000–1016 (2012).
6. Billiet, T. *et al.* Age-related microstructural differences quantified using myelin water imaging and advanced diffusion MRI. *Neurobiol. Aging* **36**, 2107–2121 (2015).
7. Chang, Y. S. *et al.* White Matter Changes of Neurite Density and Fiber Orientation Dispersion during Human Brain Maturation. *PLOS ONE* **10**, e0123656 (2015).
8. Eaton-Rosen, Z. *et al.* Longitudinal measurement of the developing grey matter in preterm subjects using multi-modal MRI. *NeuroImage* **111**, 580–589 (2015).
9. Genc, S., Malpas, C. B., Holland, S. K., Beare, R. & Silk, T. J. Neurite density index is sensitive to age related differences in the developing brain. *NeuroImage* **148**, 373–380 (2017).
10. Kodiweera, C., Alexander, A. L., Harezlak, J., McAllister, T. W. & Wu, Y.-C. Age effects and sex differences in human brain white matter of young to middle-aged adults: A DTI, NODDI, and q-space study. *NeuroImage* **128**, 180–192 (2016).
11. Kunz, N. *et al.* Assessing white matter microstructure of the newborn with multi-shell diffusion MRI and biophysical compartment models. *NeuroImage* **96**, 288–299 (2014).
12. Adluru, G. *et al.* Assessment of white matter microstructure in stroke patients using NODDI. in 742–745 (IEEE, 2014). doi:10.1109/EMBC.2014.6943697
13. Billiet, T. *et al.* Characterizing the microstructural basis of "unidentified bright objects" in neurofibromatosis type 1: A combined in vivo multicomponent T2 relaxation and multi-shell diffusion MRI analysis. *NeuroImage Clin.* **4**, 649–658 (2014).
14. Timmers, I. *et al.* White matter microstructure pathology in classic galactosemia revealed by neurite orientation dispersion and density imaging. *J. Inherit. Metab. Dis.* **38**, 295–304 (2015).
15. Dowell, N. G. *et al.* Interferon-alpha-Induced Changes in NODDI Predispose to the Development of Fatigue. *Neuroscience* (2017). doi:10.1016/j.neuroscience.2017.12.040

bioRxiv preprint doi: https://doi.org/10.1101/441659; this version posted August 5, 2019. The copyright holder for this preprint (which was not certified by peer review) is the author/funder, who has granted bioRxiv a license to display the preprint in perpetuity. It is made available under aCC-BY-NC-ND 4.0 International license.

16. Song, Y. *et al.* A study of neurite orientation dispersion and density imaging in wilson's disease: NODDI Application in Wilson's Disease. *J. Magn. Reson. Imaging* (2017). doi:10.1002/jmri.25930

17. Winston, G. P. *et al.* Advanced diffusion imaging sequences could aid assessing patients with focal cortical dysplasia and epilepsy. *Epilepsy Res.* **108**, 336–339 (2014).

18. Nazeri, A. *et al.* Functional Consequences of Neurite Orientation Dispersion and Density in Humans across the Adult Lifespan. *J. Neurosci.* **35**, 1753–1762 (2015).

19. Nazeri, A. *et al.* Gray Matter Neuritic Microstructure Deficits in Schizophrenia and Bipolar Disorder. *Biol. Psychiatry* (2016). doi:10.1016/j.biopsych.2016.12.005

20. Fukutomi, H. *et al.* Neurite imaging reveals microstructural variations in human cerebral cortical gray matter. *NeuroImage* **182**, 488–499 (2018).

21. Glasser, M. F. & Van Essen, D. C. Mapping human cortical areas in vivo based on myelin content as revealed by T1- and T2-weighted MRI. *J. Neurosci. Off. J. Soc. Neurosci.* **31**, 11597–11616 (2011).

22. *Cellular Structure of the Human Cerebral Cortex: Translated and edited by L.C. Triarhou (Thessaloniki) Plus poster: 'The 107 Cortical Cytoarchitectonic Areas of Constantin von Economo and Georg N. Koskinas in the Adult Human Brain'*. (S. Karger AG, 2009). doi:10.1159/isbn.978-3-8055-9062-4

23. von Economo, C. & Koskinas. *Die Cytoarchitektonik der Hirnrinde des erwachsenen Menschen. Textband. Verlag von Julius Springer, Berlin*. (1925).

24. Lampinen, B. *et al.* Neurite density imaging versus imaging of microscopic anisotropy in diffusion MRI: A model comparison using spherical tensor encoding. *NeuroImage* **147**, 517–531 (2017).

25. Grussu, F. *et al.* Neurite dispersion: a new marker of multiple sclerosis spinal cord pathology? *Ann. Clin. Transl. Neurol.* **4**, 663–679 (2017).

26. Sato, K. *et al.* Understanding microstructure of the brain by comparison of neurite orientation dispersion and density imaging (NODDI) with transparent mouse brain. *Acta Radiol. Open* **6**, 205846011770381 (2017).

27. Schilling, K. G. *et al.* Histological validation of diffusion MRI fiber orientation distributions and dispersion. *NeuroImage* **165**, 200–221 (2018).

28. Mollink, J. *et al.* Evaluating fibre orientation dispersion in white matter: Comparison of diffusion MRI, histology and polarized light imaging. *NeuroImage* **157**, 561–574 (2017).

29. Kamagata, K. *et al.* Gray Matter Abnormalities in Idiopathic Parkinson's Disease: Evaluation by Diffusional Kurtosis Imaging and Neurite Orientation Dispersion and Density

bioRxiv preprint doi: https://doi.org/10.1101/441659; this version posted August 5, 2019. The copyright holder for this preprint (which was not certified by peer review) is the author/funder, who has granted bioRxiv a license to display the preprint in perpetuity. It is made available under aCC-BY-NC-ND 4.0 International license.

Imaging: Gray Matter Abnormalities in Parkinson's Disease. *Hum. Brain Mapp.* (2017). doi:10.1002/hbm.23628

30. Wang, Z. *et al.* A study of neurite orientation dispersion and density imaging in ischemic stroke. *Magn. Reson. Imaging* **57**, 28–33 (2019).

31. Assaf, Y. & Cohen, Y. Assignment of the water slow-diffusing component in the central nervous system using q-space diffusion MRS: Implications for fiber tract imaging. *Magn. Reson. Med.* **43**, 191–199 (2000).

32. DeLano, M. C., Cooper, T. G., Siebert, J. E., Potchen, M. J. & Kuppusamy, K. High-b-value Diffusion-weighted MR Imaging of Adult Brain: Image Contrast and Apparent Diffusion Coefficient Map Features. *Am. J. Neuroradiol.* **21**, 1830–1836 (2000).

33. Dudink, J. *et al.* High b-Value Diffusion Tensor Imaging of the Neonatal Brain at 3T. *Am. J. Neuroradiol.* **29**, 1966–1972 (2008).

34. Baumann, P. S. *et al.* High b-value diffusion-weighted imaging: A sensitive method to reveal white matter differences in schizophrenia. *Psychiatry Res. Neuroimaging* **201**, 144–151 (2012).

35. Hagmann, P. *et al.* White matter maturation reshapes structural connectivity in the late developing human brain. *Proc. Natl. Acad. Sci.* **107**, 19067–19072 (2010).

36. Edwards, L. J., Pine, K. J., Ellerbrock, I., Weiskopf, N. & Mohammadi, S. NODDI-DTI: Estimating Neurite Orientation and Dispersion Parameters from a Diffusion Tensor in Healthy White Matter. *Front. Neurosci.* **11**, (2017).

37. Glasser, M. F. *et al.* The minimal preprocessing pipelines for the Human Connectome Project. *NeuroImage* **80**, 105–124 (2013).

38. Sotiropoulos, S. N. *et al.* Advances in diffusion MRI acquisition and processing in the Human Connectome Project. *NeuroImage* **80**, 125–143 (2013).

39. Jensen, J. H., Helpern, J. A., Ramani, A., Lu, H. & Kaczynski, K. Diffusional kurtosis imaging: The quantification of non-gaussian water diffusion by means of magnetic resonance imaging. *Magn. Reson. Med.* **53**, 1432–1440 (2005).

40. Daducci, A. *et al.* Accelerated Microstructure Imaging via Convex Optimization (AMICO) from diffusion MRI data. *NeuroImage* **105**, 32–44 (2015).

41. Glasser, M. F. *et al.* A multi-modal parcellation of human cerebral cortex. *Nature* **536**, 171–178 (2016).

42. Robinson, E. C. *et al.* Multimodal surface matching with higher-order smoothness constraints. *NeuroImage* **167**, 453–465 (2018).

43. Robinson, E. C. *et al.* MSM: a new flexible framework for Multimodal Surface Matching

bioRxiv preprint doi: https://doi.org/10.1101/441659; this version posted August 5, 2019. The copyright holder for this preprint (which was not certified by peer review) is the author/funder, who has granted bioRxiv a license to display the preprint in perpetuity. It is made available under aCC-BY-NC-ND 4.0 International license.

☆. *NeuroImage* **100**, 414 (2014).

44. Marcus, D. S. *et al.* Human Connectome Project informatics: Quality control, database services, and data visualization. *NeuroImage* **80**, 202–219 (2013).

45. Bland, J. M. & Altman, DouglasG. STATISTICAL METHODS FOR ASSESSING AGREEMENT BETWEEN TWO METHODS OF CLINICAL MEASUREMENT. *The Lancet* **327**, 307–310 (1986).

46. Whittall, K. P. *et al.* In vivo measurement ofT2 distributions and water contents in normal human brain. *Magn. Reson. Med.* **37**, 34–43 (1997).

47. Beaulieu, C. & Allen, P. S. Water diffusion in the giant axon of the squid: Implications for diffusion‐weighted MRI of the nervous system. *Magn. Reson. Med.* **32**, 579–583 (1994).

48. Hui, E. S., Cheung, M. M., Chan, K. C. & Wu, E. X. B-value dependence of DTI quantitation and sensitivity in detecting neural tissue changes. *NeuroImage* **49**, 2366–2374 (2010).

49. Farrell, J. A. D. *et al.* Effects of signal-to-noise ratio on the accuracy and reproducibility of diffusion tensor imaging–derived fractional anisotropy, mean diffusivity, and principal eigenvector measurements at 1.5T. *J. Magn. Reson. Imaging* **26**, 756–767 (2007).

50. Jones, D. K. & Basser, P. J. ?Squashing peanuts and smashing pumpkins?: How noise distorts diffusion-weighted MR data. *Magn. Reson. Med.* **52**, 979–993 (2004).

51. Burdette, J. H., Durden, D. D., Elster, A. D. & Yen, Y. F. High b-value diffusion-weighted MRI of normal brain. *J. Comput. Assist. Tomogr.* **25**, 515–519 (2001).

52. Papadakis, N. G. *et al.* A study of rotationally invariant and symmetric indices of diffusion anisotropy. *Magn. Reson. Imaging* **17**, 881–892 (1999).

53. Grussu, F., Schneider, T., Zhang, H., Alexander, D. C. & Kingshott, C. A. M. W. Neurite orientation dispersion and density imaging of the healthy cervical spinal cord in vivo. *NeuroImage* **111**, 590–601 (2015).

54. Mah, A., Geeraert, B. & Lebel, C. Detailing neuroanatomical development in late childhood and early adolescence using NODDI. *PLOS ONE* **12**, e0182340 (2017).

55. Batalle, D. *et al.* Different patterns of cortical maturation before and after 38 weeks gestational age demonstrated by diffusion MRI in vivo. *NeuroImage* **185**, 764–775 (2019).

56. Colgan, N. *et al.* Application of neurite orientation dispersion and density imaging (NODDI) to a tau pathology model of Alzheimer's disease. *NeuroImage* **125**, 739–744 (2016).

57. Jones, D. K. The effect of gradient sampling schemes on measures derived from diffusion tensor MRI: A Monte Carlo study. *Magn. Reson. Med.* **51**, 807–815 (2004).

58. Chou, M.-C. *et al.* FLAIR Diffusion-Tensor MR Tractography: Comparison of Fiber Tracking with Conventional Imaging. *Am. J. Neuroradiol.* **26**, 591–597 (2005).

bioRxiv preprint doi: https://doi.org/10.1101/441659; this version posted August 5, 2019. The copyright holder for this preprint (which was not certified by peer review) is the author/funder, who has granted bioRxiv a license to display the preprint in perpetuity. It is made available under aCC-BY-NC-ND 4.0 International license.

59. Kwong, K. K. *et al.* CSF-suppressed quantitative single-shot diffusion imaging. *Magn. Reson. Med.* **21**, 157–163 (1991).

60. Jelescu, I. O., Veraart, J., Fieremans, E. & Novikov, D. S. Degeneracy in model parameter estimation for multi-compartmental diffusion in neuronal tissue: Degeneracy in Model Parameter Estimation of Diffusion in Neural Tissue. *NMR Biomed.* **29**, 33–47 (2016).

61. Jespersen, S. N. *et al.* Neurite density from magnetic resonance diffusion measurements at ultrahigh field: comparison with light microscopy and electron microscopy. *NeuroImage* **49**, 205–216 (2010).

62. Schmierer, K. *et al.* Diffusion tensor imaging of post mortem multiple sclerosis brain. *Neuroimage* **35**, 467–477 (2007).

63. Rosenberg, G. A., Kyner, W. T. & Estrada, E. Bulk flow of brain interstitial fluid under normal and hyperosmolar conditions. *Am. J. Physiol.-Ren. Physiol.* **238**, F42–F49 (1980).

64. Lanzafame, S. *et al.* Differences in Gaussian diffusion tensor imaging and non-Gaussian diffusion kurtosis imaging model-based estimates of diffusion tensor invariants in the human brain: Model-based differences in diffusion tensor invariants. *Med. Phys.* **43**, 2464–2475 (2016).

Table 1

Abbreviations of b-shell datasets	Datasets of non-diffusion weighted (b=0) and diffusion-weighted MRI volumes (b=1000,2000 and 3000)
b_{1000}	b=0 (18), b=1000 (90)
b_{2000}	b=0 (18), b=2000 (90)
b_{3000}	b=0 (18), b=3000 (90)
$b_{1000\text{-}2000}$	b=0 (18), b=1000 (90), b=2000 (90)
$b_{1000\text{-}3000}$	b=0 (18), b=1000 (90), b=3000 (90)
$b_{2000\text{-}3000}$	b=0 (18), b=2000 (90), b=3000 (90)
b_{All}	b=0 (18), b=1000 (90), b=2000 (90), b=3000 (90)

Legends

Table 1

The table lists abbreviations of b-shell datasets used in the main text and corresponding datasets of dMRI in different b-shell schemes. The numbers in parentheses indicate the number of b0 volumes with repeatedly obtained for b=0 volume or diffusion weighted directions with different b-vectors (or directions of diffusion-weighted gradient) for each of the b=1000, 2000 and 3000 shells.

bioRxiv preprint doi: https://doi.org/10.1101/441659; this version posted August 5, 2019. The copyright holder for this preprint (which was not certified by peer review) is the author/funder, who has granted bioRxiv a license to display the preprint in perpetuity. It is made available under aCC-BY-NC-ND 4.0 International license.

Figure 1. Relationships of DTI and NODDI when assumed non-CSF compartment. The equations for DTI-derived NODDI calculation (Eq. 2-5) and d// =1.1×10-3 mm2/s (optimized for gray matter) were used to simulate relationships between (A) Neurite density index (NDI) vs inversed mean diffusivity (1/MD), over the range of MD= 1500 to 2000 s/mm2, and (B) orientation dispersion index (ODI) vs MD when fractional anisotropy (FA) ranged from 0.1 to 0.6. Details of derivation of mathematical function of DTI and NODDI are described in Supplementary text 1.2.

Figure 2. Cross-subject average cortical surface maps of neurite density index (NDI) and mean diffusivity (MD).
Cortical surfaces are different in terms of computation methods: original NODDI NDI (NDIORIG) (A, D, G), DTI-derived MD (B, E, H) and DTI-derived NODDI NDI (NDIDTI) (C, F, I) with different b-shell datasets used: all three b-values (bAll), only those of b=3000 (b3000) and b=1000 (b1000), respectively. Reference cortical surface maps of NDIORIG with bAll in (A) showed high values in primary sensorimotor, visual, auditory cortices as well as the middle temporal (MT) area, similar to the cortical myelin distribution as reported previously20. Both MD/bAll and MD/b3000 (B, E) showed inversed appearance to the reference, as well as both NDIDTI/bAll and NDIDTI/b3000 (C, F) showed very similar surface distribution to the reference. Note that NDIORIG/b3000 in (D) showed a different pattern from the reference and any computation methods using b1000 (G, H, I) did not show comparable pattern with the reference. https://balsa.wustl.edu/L66BP

Figure 3. Cross-subject average cortical surface maps of orientation dispersion index (ODI) and fractional anisotropy (FA).
Cortical surfaces are different in terms of computation methods: original NODDI ODI (ODIORIG) (A, D, G), DTI-derived FA (B, E, H) and DTI-derived NODDI ODI (ODIDTI) (C, F, I), each used different b-shell datasets: all three b-values (bAll) vs only those of b=3000 (b3000) and low b-values (b1000), respectively. A reference cortical map of ODI (ODIORIG/bAll) in (A) showed high values in the early sensory areas including somatosensory, auditory, and visual. Note that ODIORIG/b3000, ODIDTI/bAll in (C) and ODIDTI/b3000 in (F) showed similar distribution to the reference. Any computation methods using b1000 (H, I, J) did not show comparable pattern with the reference. Data at https://balsa.wustl.edu/pkkKj

Figure 4. Correlation coefficients of DTI-derived parameters (MD and FA) and DTI-derived NODDI parameters (NDIDTI and ODIDTI) with the references that are the original NODDI parameters on three-shell dataset (NDIORIG/bAll and ODIORIG/bAll). Correlation coefficients to the references

bioRxiv preprint doi: https://doi.org/10.1101/441659; this version posted August 5, 2019. The copyright holder for this preprint (which was not certified by peer review) is the author/funder, who has granted bioRxiv a license to display the preprint in perpetuity. It is made available under aCC-BY-NC-ND 4.0 International license.

were calculated using averaged surface maps across all subjects in each different b-shell dataset type (b1000, b2000, b3000, b1000-2000, b1000-3000, b2000-3000 and bAll). All correlations were significant ($p<0.00001$).

Figure 5. Bland-Altman plots between DTI-derived NODDI and original NODDI parameters in vivo. (A and C) show Bland-Altman plots between DTI-derived NODDI parameters in the three -shell dataset (bAll) and the original NODDI parameters in the three-shell dataset (bAll). (B and D) show Bland-Altman plots between DTI-derived NODDI parameters in the high b-value one-shell dataset (b3000) and the original NODDI parameters in the three-shell dataset (bAll). Plots are coloured by their density. Blue lines show the mean±1.96*SD and the red line shows the mean value. Abbreviations; NDIORIG: neurite density index estimated using the original NODDI model, ODIORIG: orientation dispersion index estimated using the original NODDI model, NDIDTI: neurite density index estimated using DTI-derived NODDI, ODIDTI: orientation dispersion index estimated using DTI-derived NODDI.

Figure 6. Results of simulation for percent errors in DTI-derived parameters depending on various range of the CSF volume fraction. A) The percent errors in NDI in NODDI (%ΔNDIORIG, left panel), DTI MD (%ΔMD, middle panel) and DTI-derived NDI (%ΔNDIDTI, right panel) against various levels of CSF volume fraction (Viso) relative to the refence value (=0.1). B) The percent errors in ODI from the NODDI (%ΔODIORIG, left panel), DTI FA (%ΔFA, middle) and DTI-derived ODI (%ΔODIDTI, right panel). Dataset types of b-shell schemes b1000, b2000, b3000, b1000-2000, b1000-3000, b2000-3000 and bAll are shown in different colored lines as in the legend in each panel. Note that the one-shell low b-value data set (b1000) shows the largest size of errors in DTI and DTI-derived NODDI parameters among all the datasets, which suggests high sensitivity to partial volume effects in the cortical gray matter. The smallest change in DTI-derived NODDI and DTI parameters was found when using the three-shell dMRI data (bAll), followed by the high b-value two-shell (b1000-3000) and one-shell dMRI data (b3000). Abbreviations; NDIORIG: original NODDI neurite density index, ODIORIG: original NODDI orientation dispersion index, NDIDTI: DTI-derived NODDI neurite density index, ODIDTI: DTI-derived NODDI orientation dispersion index

bioRxiv preprint doi: https://doi.org/10.1101/441659; this version posted August 5, 2019. The copyright holder for this preprint (which was not certified by peer review) is the author/funder, who has granted bioRxiv a license to display the preprint in perpetuity. It is made available under aCC-BY-NC-ND 4.0 International license.

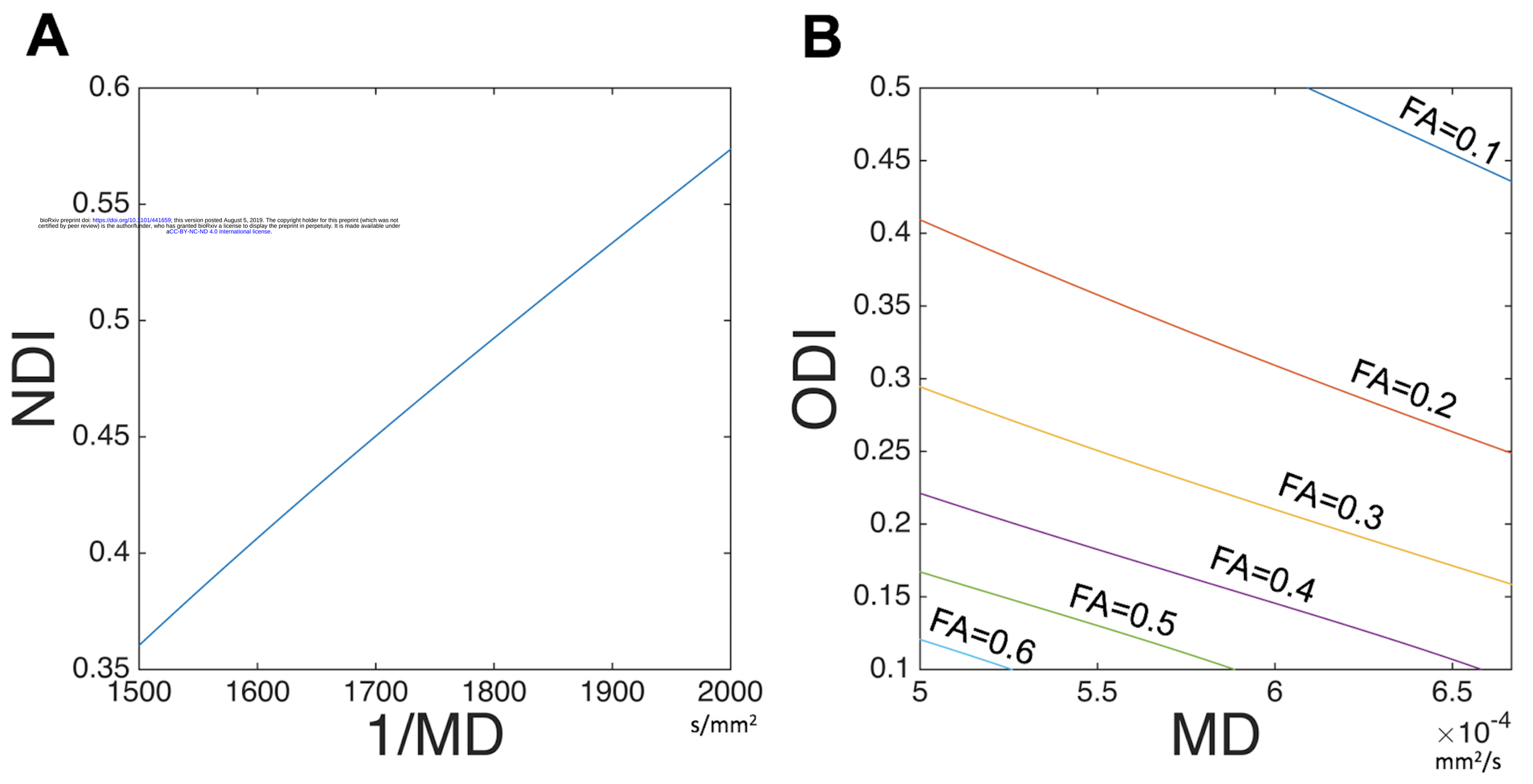

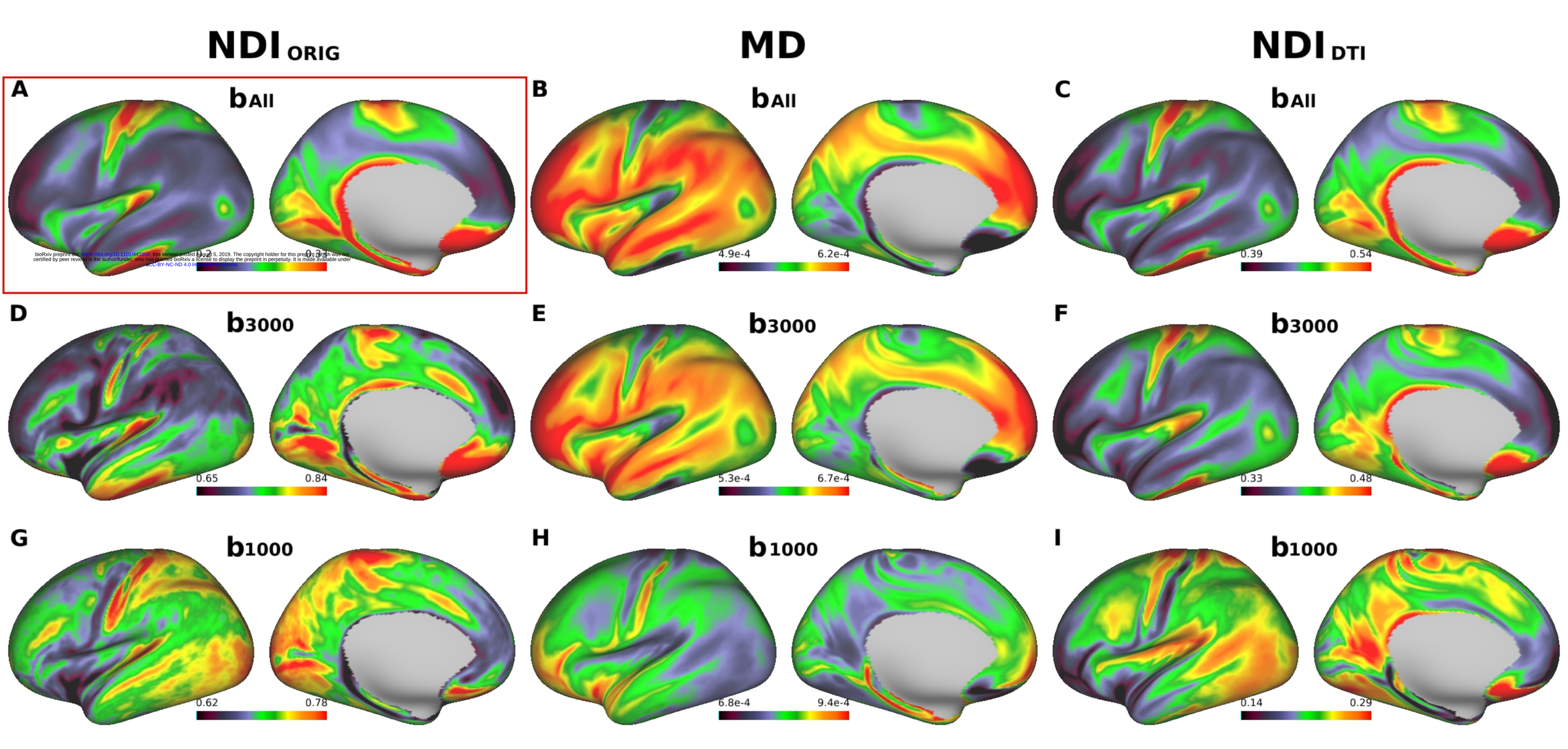

bioRxiv preprint doi: https://doi.org/10.1101/441956; this version posted August 5, 2019. The copyright holder for this preprint (which was not certified by peer review) is the author/funder, who has granted bioRxiv a license to display the preprint in perpetuity. It is made available under CC-BY-NC-ND 4.0 International license.

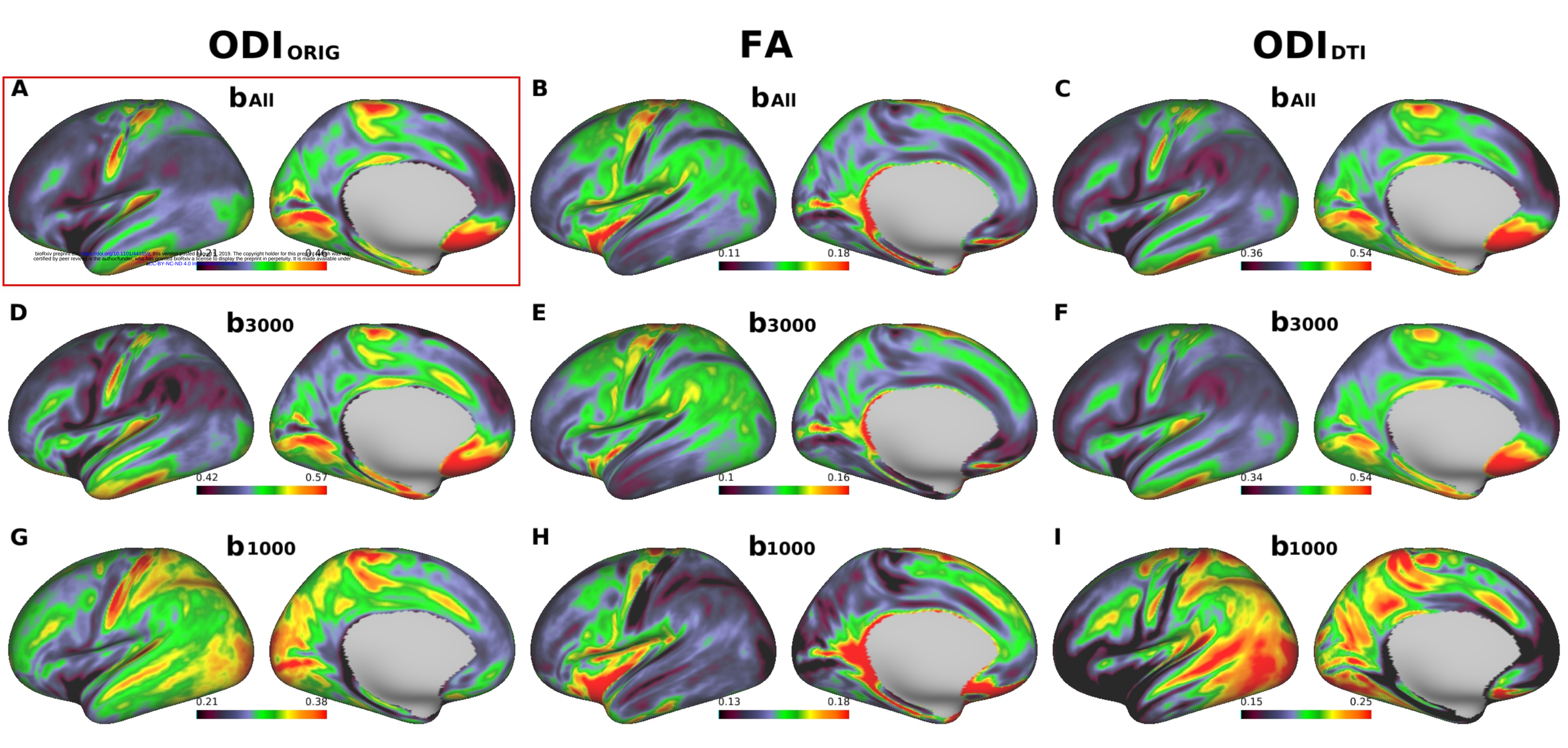

bioRxiv preprint doi: https://doi.org/10.1101/441659; this version posted August 1, 2019. The copyright holder for this preprint (which was not certified by peer review) is the author/funder, who has granted bioRxiv a license to display the preprint in perpetuity. It is made available under CC-BY-NC-ND 4.0 International license.

bioRxiv preprint doi: https://doi.org/10.1101/441865 posted August 5, 2019. The copyright holder for this preprint (which was not peer review) is the author/funder. It is made available under a license to display the preprint in perpetuity. It is made available under CC BY-NC-ND 4.0 International license.

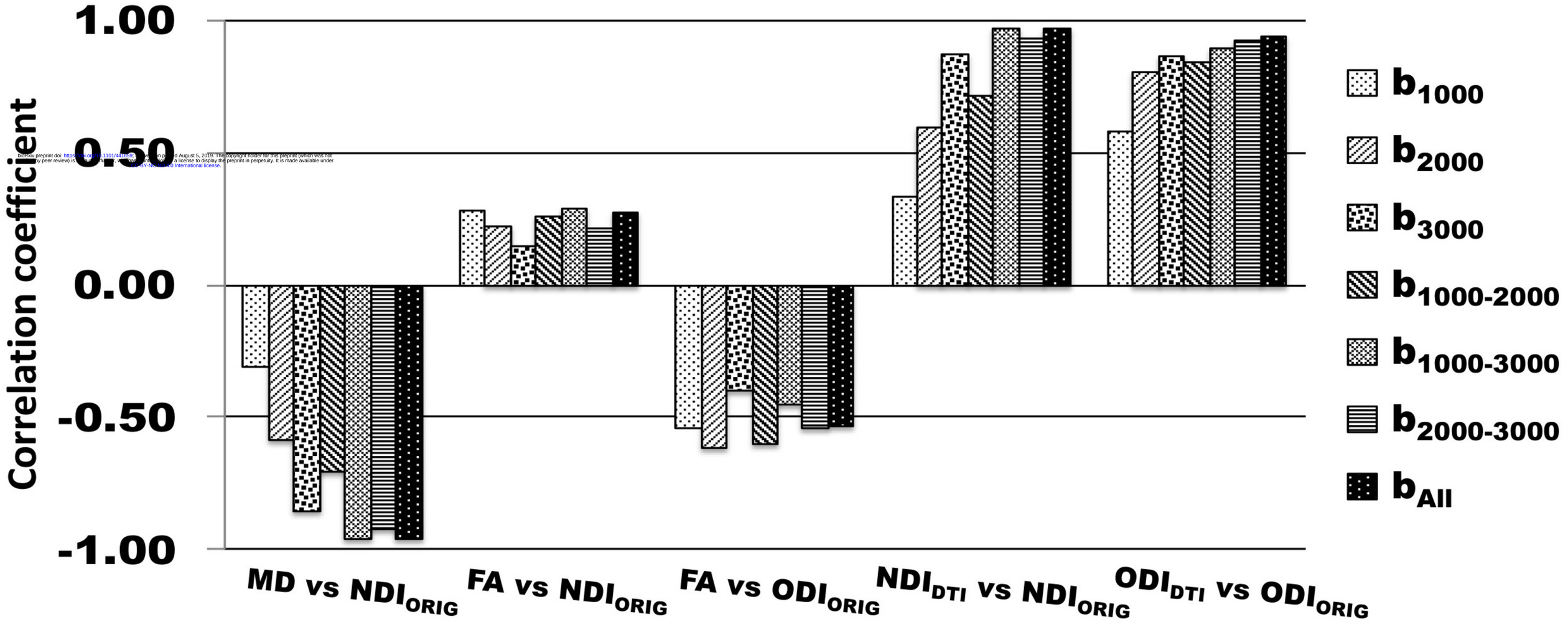

A

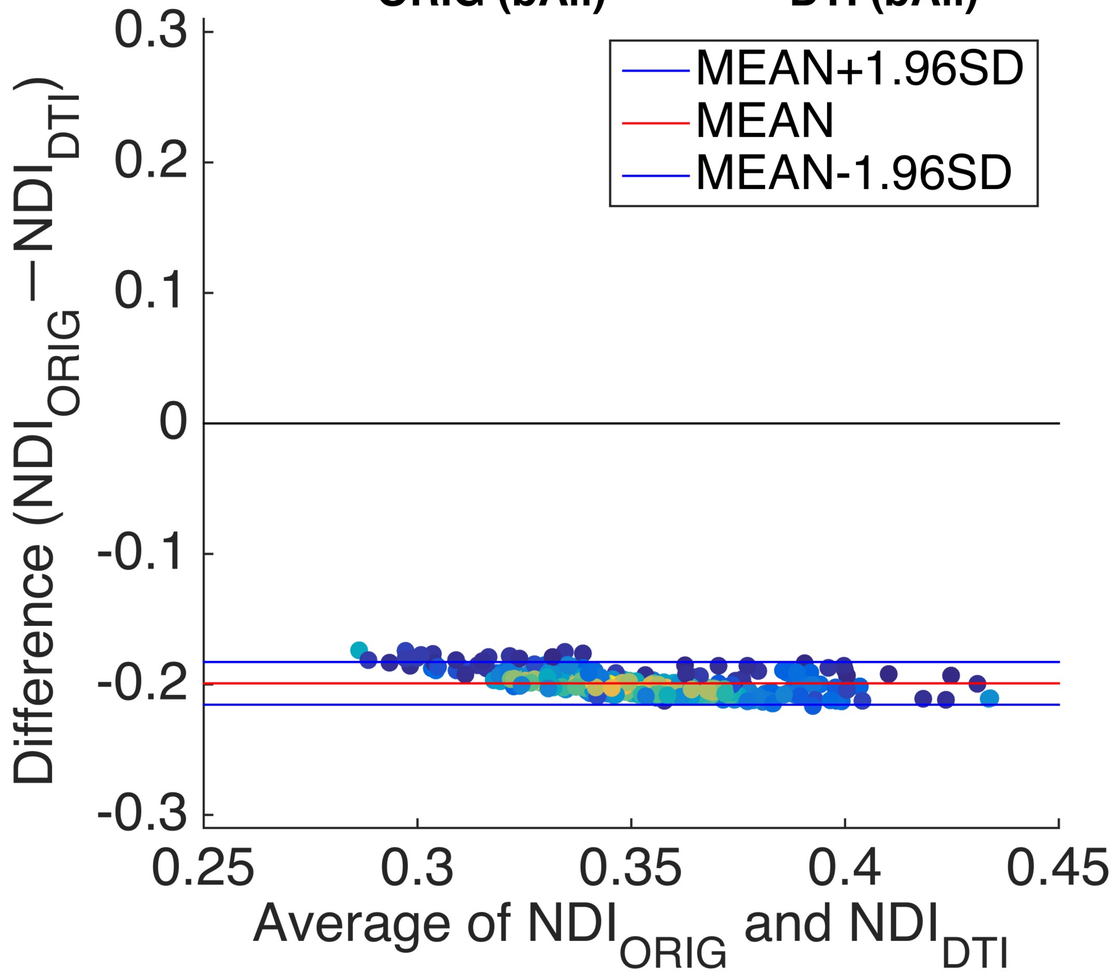

B

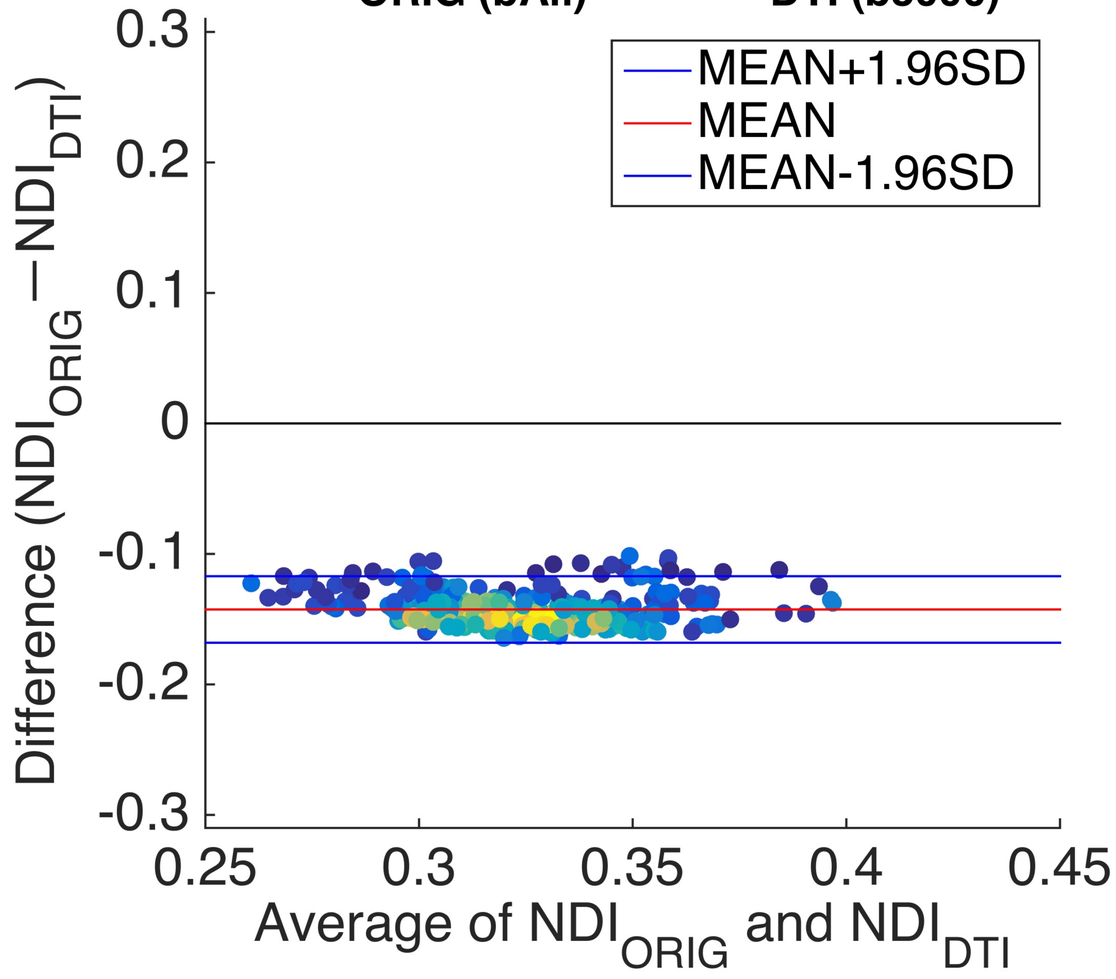

C

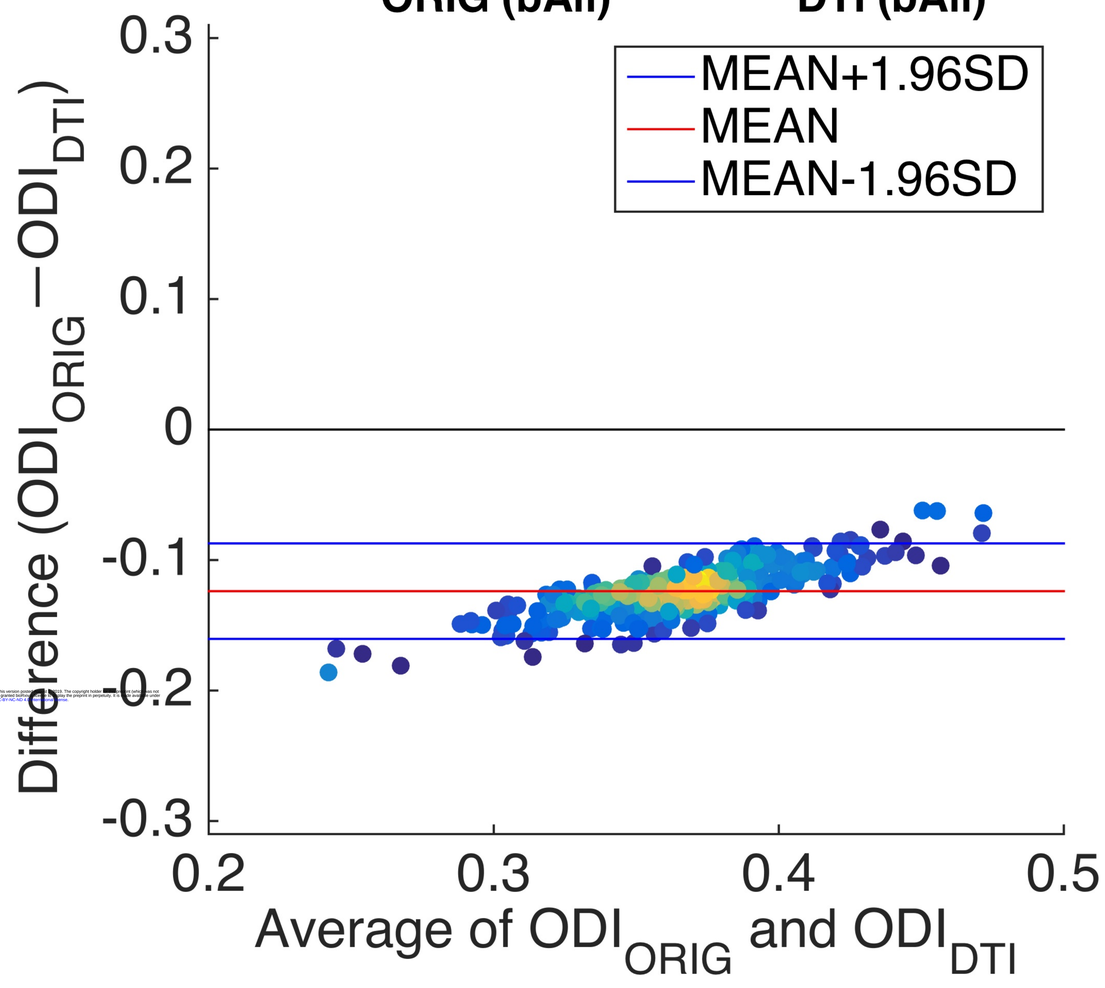

D

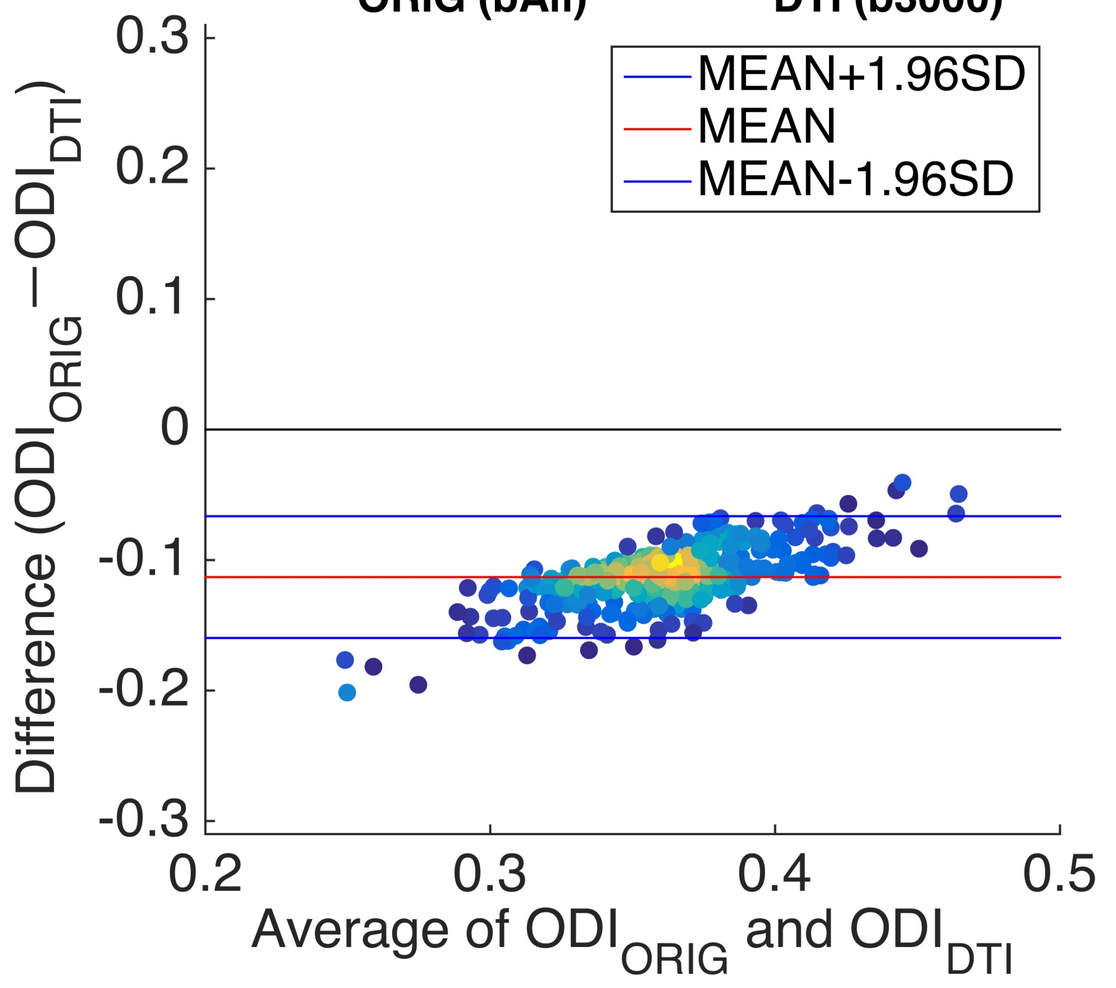

bioRxiv preprint doi: https://doi.org/10.1101/443955; this version posted October 8, 2018. The copyright holder for this preprint (which was not certified by peer review) is the author/funder, who has granted bioRxiv a license to display the preprint in perpetuity. It is made available under aCC-BY-NC-ND 4.0 International license.

bioRxiv preprint doi: https://doi.org/10.1101/441659; this version posted August 5, 2019. The copyright holder for this preprint (which was not certified by peer review) is the author/funder, who has granted bioRxiv a license to display the preprint in perpetuity. It is made available under aCC-BY-NC-ND 4.0 International license.